ASYMMETRY OF NONLINEAR SOIL STRAINS DURING SOIL-STRUCTURE INTERACTION EXCITED BY SH PULSE

ASIMETRIJA U NELINEARNIM DEFORMACIJAMA TLA ZA VREME INTERAKCIJE TLO-KONSTRUKCIJA POBUĐENE PULSOM SH TALASA

UDK:
Kakav rad

Prof. Vlado GIČEV, Ph. D., Civ. Eng.[1],
Prof. Mihailo D. TRIFUNAC, Ph. D., Civ. Eng.[2]

SUMMARY

A two-dimensional (2D) model of a building supported by a rectangular, flexible foundation embedded in nonlinear soil is analyzed. The model is excited by a half-sine SH wave pulse, which travels towards the foundation. The results show that the spatial distribution of permanent, nonlinear strain in the soil depends upon the incident angle, the amplitude, and the duration of the pulse. If the wave has large amplitude and short duration, the nonlinear zone in the soil appears immediately or after the reflection from the half-space, in which case it is located close to the free surface. This results from interference of the reflected pulse from the free surface and the incoming part of the pulse that still has not reached the free surface. The work spent for the development of nonlinear strains in the soil can consume a significant part of the input wave energy, and thus less energy is available for excitation of the building.

Key words: *soil-structure interaction: nonlinear waves in the soil; distribution of wave energy.*

REZIME

U ovom radu je analiziran dvodimenzionalni (2D) model konstrukcije na pravougaonom elastičnom fundamentu, ukopanom u tlo sa nelinearnim osobinama. Pobuđenje modela je polusinusoidnim pulsom SH talasa koji se prostire prema fundamentu. Rezultati pokazuju da prostorni raspored nelinearnih deformacija u tlu zavisi od ulaznog ugla, amplitude i trajanja pulsa. Ako puls ima veliku amplitudu a kratko trajanje, nelinearne zone u tlu se pojavljuju odmah ili posle odbijanja talasa od površine poluprostora, i u tom slučaju se javljaju blizu površine. Te nelinearne zone su posledica interferencije odbijenog pulsa od površine polu-prostora i pristižućeg dela pulsa koji još nije stigao do površine. Rad utrošen na formiranju nelinearnih deformacija u tlu može da utroši značajan deo ulazne energije i time je energija koja preostaje za pobuđenje odgovora konstrukcije znatno umanjena.

Ključne reči: *interakcija tlo-konstrukcija; nelinearni talasi u tlu; raspored talasne energije.*

INTRODUCTION

There is ample observational evidence that soil response can become highly nonlinear in the near-field of strong earthquakes. This is manifested by the visible effects on the ground surface, by the damage to water and gas pipes (Trifunac & Todorovska 1997a,b), by the characteristic changes in the recorded time series of strong ground motion (Trifunac & Todorovska 1996; Trifunac & Ivanović 2003a,b; Trifunac et al. 1999a), and by the changes in the structural response (Luco et al. 1987; Trifunac et al. 1999b; 2001a,b). Field reconnaissance of the effects of many earthquakes has provided numerous examples of different types of soil failure and permanent deformations caused by strong shaking (Duke 1958; Kanai 1983). Examples include settlement of cohesionless soils, liquefaction of saturated sands, flow slides due to liquefaction of cohesionless soils, bulkhead failures due to backfill liquefaction, slides caused by liquefaction of thin sand layers, failures of piles on weak foundations, and lateral movement of bridge abutments. Many structures settle, tilt, or overturn on liquefied soil. Some of the best-known examples of this occurred during the 1964 Alaska and 1964 Niigata earthquakes (Seed, 1970).

Nonlinear soil response adds numerous complexities to the soil and structural response above and under the ground surface (Trifunac and Lee 1996; Trifunac et al.

Adresa autora: [1] Univ. Goce Delčev, Dept. of Computer Science, Tošo Arsov 14, 2000 Štip, R. Macedonia
[2] Univ. Southern California, Dept. of Civil Eng., Los Angeles, California 90089-2531, USA
E-mail: vlado.gicev@ugd.edu.mk
trifunac@usc.edu

1996). It alters and redistributes the spectral amplitudes relative to what is recorded at intermediate and large distances from the source and alters the distributions of the peaks of structural response (Udwadia and Trifunac 1974). Spatial variations in the permanent post-earthquake soil deformations can lead to significant increases in pseudo static loads, especially for long and extended structures (Trifunac and Todorovska 1997c, Todorovska and Trifunac 1989; Trifunac and Gičev 2006), and must be added to the estimates of the permanent movement of the foundations caused by faulting (Todorovska et al. 2007). While for structures with small plan dimensions the energy absorbed by the nonlinear site response can lead to a significant reduction of the energy arriving from the earthquake source (Trifunac 2008), thus reducing the damaging characteristics of strong motion (Trifunac and Todorovska 1999), for large and extended structures the transient and permanent displacements and rotations can lead to significantly larger overall forces in the structures.

The sequence of the soil-structure interaction (SSI) phenomena, like the one that led to the overturning of apartment buildings in Kawagishi-cho during the Niigata earthquake (Seed 1970), is complicated, and its modelling and analysis still present a major challenge for any nonlinear numerical simulation. It probably started with development of nonlinear strain zones in the soil close to the foundation, associated with large power carried by the incident seismic waves, which initiated liquefaction (Trifunac 1995), which then spread all around the foundation, causing the buildings to tilt and overturn. Analysis of this entire sequence is well beyond the scope of this paper, but we can explore the early stages, which involve creation of the nonlinear zones in the soil.

Analytical studies have been conducted to analyse the influence of the shape of a rigid foundations and of interaction of several rigid foundations (Wong and Trifunac 1975). Wong and Trifunac (1974) solved the interaction of the shear wall on an elliptical, rigid foundation for shallow and deep embedment, and Westermo and Wong (1977) studied different boundary models for the soil-structure interaction of an embedded, semi-circular, rigid foundation. They concluded that without a transmitting boundary all of the models develop resonant behaviour and that the introduced damping in the soil cannot adequately model the radiation damping. Luco and Wong (1977) studied a rectangular foundation welded to an elastic half-space and excited by a horizontally propagating Rayleigh wave. Lee (1979) solved a 3D interaction problem consisting of a single mass supported by an embedded, hemispherical, rigid foundation for incident plane P, SV, and SH waves in spherical coordinates. In recent publications, which deal with a flexible foundation, Todorovska et al. (2001) analysed interaction of a dike on a flexible, embedded foundation, and Hayir et al. (2001) described the same dike, but in the absence of a foundation. Aviles et al. (2002) analysed the in-plane motion of a 4-degrees-of-freedom model, and Gičev (2005; 2008) studied the soil-flexible foundation-structure interaction for incident-plane SH waves with a numerical model using finite differences. The current paper is an extension of the work of Gicev (2008) to the case of rectangular embedded foundation.

The purpose of this paper is to show how the nonlinear strain localization occurs in asymmetric fashion around the foundation when incident seismic waves arrive with non-vertical incidence. This asymmetry will contribute to more prominent wave-passage effects, which in turn will lead to more powerful rocking excitation of the embedded foundation, and for the case of in-plane excitation it may subsequently lead to overturning of the structure.

The linear soil-structure interaction phenomenon includes several features, among them wave scattering, radiation damping, damping in the structure, and the presence of different frequencies (system frequency, apparent frequency, rocking frequency, horizontal frequency, and fixed-base frequency; Todorovska 2009). In this paper, in the presence of the interaction, the development of the nonlinear zones in the soil is studied for incident pulses representing the near-field destructive strong ground motion. The problems that must be addressed in the numerical study of the nonlinear soil-structure interaction include heterogeneities and discontinuities in the medium, the modelling of the free surface, transmitting boundaries, and keeping track of the nonlinear constitutive law at each point in the soil. The lessons learned from such nonlinear analysis are important not only for understanding the nonlinear SSI but also for characterization of permanent deformations imposed on various underground pipes that are connected to the foundations, as in nuclear power plants, for example.

Advanced large scale numerical simulations have been developed for analyses of dynamic response of soils, including nonlinear representation and complex geometry of foundations (Cai et al. 2008; Caballero et al. 2008; Elgamal et al. 2008; Prevost 1993; Zhang et al. 2008). Large numerical models are necessary for engineering analyses in realistic setting, but detailed interpretation of some of their results becomes a challenge due to simultaneous action of their many complex features. With the aim of analysing and interpreting only a subset of the phenomena, which accompany the nonlinear response of soil in the presence of soil-structure interaction, in this paper we choose only the most elementary representation of waves in the soil, and adopt the bi-linear yielding model for the soil. In calculations based on finite differences this then enables us to study times and places where strain localizations introduce permanent deformations in the soil. Our aim is to learn how the permanent deformations in the soil contribute to the absorption of incident seismic wave energy.

According to Moczo (1989) and Zahradnik et al. (1993), the computational FD schemes that are used in applications of wave propagation can be divided into homogenous and heterogeneous. Alterman and Karal (1968) used the homogeneous formulation to solve elastic wave propagation in layered media, and Boore (1972)

proposed the heterogeneous scheme. Tsynkov (1998) reviewed the existing global and local artificial boundaries. The global boundaries are perfect absorbers, but they cannot be readily applied in "marching-in-time" procedures because of their non-locality, both in time and space. The main advantage of the local (imperfect) artificial boundaries is that they are local in space and time and are not frequency dependent.

MODEL

During the wave passage, the soil, the foundation, and the superstructure undergo nonlinear deformations, and after the motion is over they can be left with permanent strains. Because the aim of this paper is to study the nonlinear zones in the soil only—for simplicity—only the soil will be modelled as nonlinear, while the foundation and the building will be assumed to remain linear. The model is shown in Fig. 1. The incoming wave is a half-sine pulse of a plane SH wave, which is intended to represent strong motion pulses observed in the strong motion near faults (Housner and Trifunac 1967; Todorovska et al. 2009). A dimensionless frequency $\eta = 2a/\lambda = a/(\beta_s \cdot t_{d0})$ is introduced as a measure of the pulse duration (wavelength), where a is half the width of the foundation, λ is the wavelength of the incident wave, β_s is the shear-wave velocity in the soil, and t_{d0} is the duration of the pulse.

To set up the grid spacing, the pulse is analysed in space domain (s), and the displacement in the points occupied by the pulse is

$$w(s) = A \sin [\pi \cdot s/(\beta_s \cdot t_{d0})], \quad (1)$$

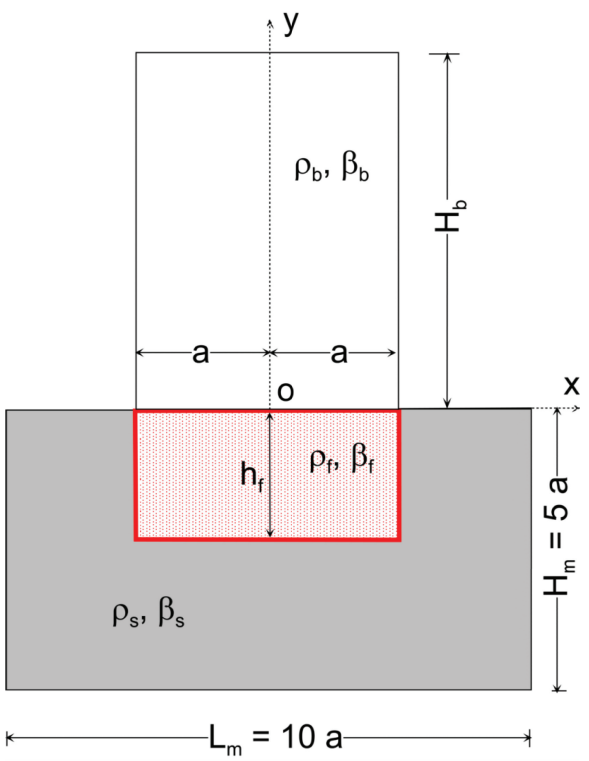

Fig. 1. Soil-flexible foundation-structure system.

where A is the amplitude of the pulse and s is the distance of the considered point to the wave front in initial time, in the direction of propagation. Using the fast Fourier transform, the half-sine pulse (Eq. 1) is transformed into wave number domain (k) as follows:

$$w(\mathrm{k}) = F\,[w(s)\,]. \quad (2)$$

The maximum response occurs for k = 0 (rigid-body motion). As k increases, the response decreases and goes asymptotically towards zero as k approaches infinity. We selected the largest wave number, $\mathrm{k} = \mathrm{k}_{max}$, for which the k-response is at least 0.03 of the maximum response (Gičev 2008). Then, for this value of k_{max}, the corresponding frequencies and the corresponding wavelengths are computed:

$$\lambda_{min} = 2\pi/\mathrm{k}_{max} = 2\pi\beta/\omega_{max} \quad (3)$$

Using the above criteria, it can be found, for example, that for $\eta = 0.5$, $\omega_{max} \approx 245$ rad/s, while for $\eta = 2$, $\omega_{max} \approx 980$ rad/s.

A measure of the numerical accuracy of the finite difference (FD) grid is related to the ratio between the numerical and physical velocities of propagation, c/β, which ideally should be 1. The parameters that influence this accuracy are:

– The density of the grid $m = \lambda/\Delta x$ (m is the number of points per wavelength λ, and Δx is the spacing between the grid points)
– The Courant number, $\chi = \beta_s\, \Delta t/\Delta x$
– The angle of the wave incidence, θ.

It has been shown by Alford et al. (1974), Dablain (1986), and Fah (1992) that the error increases when m decreases, χ decreases, and θ is close to 0 or $\pi/2$. For second-order approximation, the above authors recommend m = 12.

For relative comparisons of hysteretic energies and the nonlinear zones in the soil, the soil box should have adequate dimensions for any dimensionless frequency of the pulse, η. We chose a rectangular soil box with dimensions $\mathrm{L_m} = 10 \cdot \mathrm{a}$ and $H_m = L_m/2 = 5 \cdot a$ (Fig. 1). Also, for practical reasons, the maximum number of space intervals in the grid in the horizontal (x) direction is set at 250, and in the vertical (y) direction at 400 (125 in the soil box and 275 in the building). The minimum spatial interval for this setup is $\Delta x_{min} = L_m/250 = 95.5/250 = 0.382\ m$. For a finer grid, the computational time increases rapidly. Having this limitation in mind, from Eq. 3 and for $\eta = 2$ ($\omega_{max} = 980$ rad/s), the shortest wavelength is $\lambda_{min} = 1.603\ m$, and the finest grid density is $m = \lambda_{min}/\Delta x_{min} = 1.603/0.382 \approx 4$ points/$\lambda_{min} < m_{min}$ for this wavelength.

Our numerical scheme is $O(\Delta t^2, \Delta x^2)$, so from the above considerations we need at least m = 12 points/λ_{min} to resolve the shortest wavelength, λ_{min}. As we saw above, for $\eta = 2$ our grid cannot resolve the shortest wavelength when we have only 4 spatial grid points. This implies that the pulse should be low-pass filtered. A cut-off frequency $\omega_c = 200$ rad/s was chosen, and the pulse was low-pass filtered. This implies that $\lambda_{min} = 7.854$ m and then the grid density is

$$m = \lambda_{min}/\Delta x_{min} = 7.854/0.382 \approx$$
$$\approx 20 \text{ points}/\lambda_{min} < m_{min} \quad (4)$$

It can be shown that for $\eta = 0.5$ only a negligible amount of the total power is filtered out, while for $\eta = 2$ a considerable amount is filtered out. Also, it can be shown that for $\eta = 2$ the amplitude of the filtered pulse is smaller than the amplitude of the non-filtered pulse, which we chose to be A = 0.05 m, while for $\eta = 0.5$ the amplitude is almost equal with the amplitude of the non-filtered pulse (Gičev 2008). Our numerical tests have shown that the viscous absorbing boundary rotated towards the middle of the foundation-building interface reflects only a negligible amount of energy back into the model (Gičev 2005). For 2D problems, the numerical scheme is stable if the time increment (Mitchell 1969) is:

$$\Delta t \le \min\left[(1/\Delta x^2 + 1/\Delta y^2)^{1/2}\,\beta\right]^{-1}. \quad (5)$$

Further, we assume that the shear stress in the x direction depends only upon the shear strain in the same direction and is independent of the shear strain in the y direction (and vice versa for shear stress in the y direction). The motivation for this assumption comes from our simplified representation of layered soil, which is created by deposition (floods and wind) into more or less horizontal layers. The soil is assumed to be ideally elasto-plastic, and the constitutive σ – ε relationship is shown in Fig. 2. Further, it is assumed that the contact points between the soil and foundation remain bonded during the analysis and that the contact cells remain linear, as does the zone next to the artificial boundary (the bottom four rows and the left-most and right-most four columns in the soil box in Fig. 1).

For our problem, the system of three partial differential equations (for *u*, *v*, and *w*) describing the dynamic equilibrium of an elastic body is reduced to one equation only (because $u = v = \partial/\partial z = 0$). Neglecting the body forces in the z direction ($F_z = 0$), this equation is:

$$\rho\frac{\partial^2 w}{\partial t^2} = \left(\frac{\partial \tau_{xz}}{\partial x} + \frac{\partial \tau_{yz}}{\partial y}\right) \quad (6)$$

Introducing the new variables:

$$v = \frac{\partial w}{\partial t},\ \varepsilon_{xz} = \frac{\partial w}{\partial x},\ \text{and}\ \varepsilon_{yz} = \frac{\partial w}{\partial y}$$

and dividing (6) with ρ, the order (of 6) is reduced to the system of three first-order partial differential equations

$$\underline{U}_{,t} = \underline{F}_{,x} + \underline{G}_{,y}, \quad (7)$$

where

$$\underline{U} = \begin{Bmatrix} v \\ \varepsilon_{xz} \\ \varepsilon_{yz} \end{Bmatrix} \quad \underline{F} = \underline{F}(\underline{U}) = \begin{Bmatrix} \frac{1}{\rho}\tau_{xz} \\ v \\ 0 \end{Bmatrix} \quad \underline{G} = \underline{G}(\underline{U}) = \begin{Bmatrix} \frac{1}{\rho}\tau_{yz} \\ 0 \\ v \end{Bmatrix}. \quad (8)$$

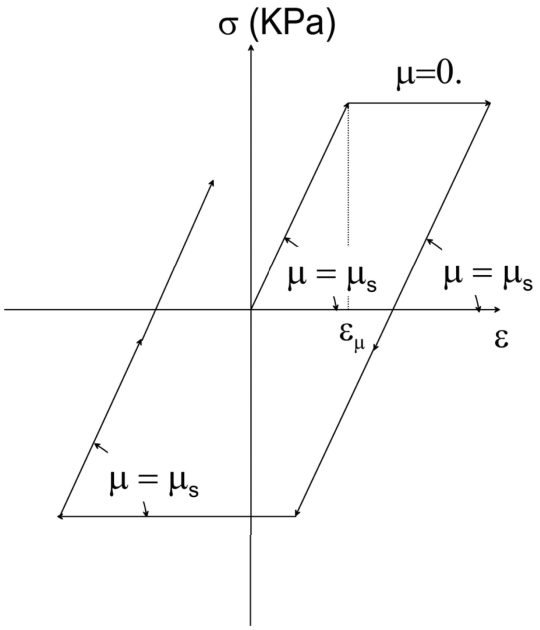

Fig. 2. The constitutive law, σ – ε, for the soil.

The first equation in (7) represents the dynamic equilibrium of forces in the z direction with neglected body force F_z, while the second and third equations give the relations between the strains and the velocity. The abbreviations $\varepsilon_x = \varepsilon_{xz}$, $\sigma_x = \tau_{xz}$, $\varepsilon_y = \varepsilon_{yz}$, and $\sigma_x = \tau_{xz}$, will be used in the text. The Lax-Wendroff computational scheme (Lax and Wendroff 1964) is used for solving Eq. (7) (Gičev 2005).

ENERGY AND PERMANENT STRAIN DISTRIBUTION

For a test example, we follow Gičev (2008) and use the properties of the Holiday Inn hotel in Van Nuys, California (Blume and Assoc. 1973), and consider the response in east-west (longitudinal) direction. This building was studied extensively using different models and representations (Gičev and Trifunac 2007; 2009; Ivanović et al. 2000; Trifunac et al. 1994; 2003), and the body of those results can be used to complement future comparisons and interpretations of its response.

A question arises as to how to choose the yielding strain ε_m (Fig. 2) to study permanent strain distribution. The displacement, the velocity, and the linear strain in the soil (β_s = 250 m/s) during the passage of a plane wave in the form of a half-sine pulse are:

$$w = A\sin\left(\pi \cdot \frac{t}{t_{d0}}\right) \quad (9)$$

$$v = \dot{w} = \left(\pi \cdot \frac{t}{t_{d0}}\right) A\cos\left(\frac{\pi t}{t_{d0}}\right) \quad (10)$$

$$|\varepsilon| = \frac{v_{max}}{\beta_s} = \frac{\pi A}{\beta_s t_{d0}} \quad (11)$$

If, for a given input plane wave, we choose the yielding strain ε_m given by (11) multiplied by some constant between 1 and 2, the strains in both directions will remain linear before the wave reaches the free surface or the foundation for any incident angle. This case can be called "intermediate nonlinearity". If we want to analyse only the nonlinearity due to scattering and radiating from the foundation, we should avoid the occurrence of the nonlinear strains caused by reflection from the half-space boundary. Then we may choose:

$$\varepsilon_m \geq \max\left(\frac{2\pi A\sin\gamma}{\beta_s t_{d0}};\frac{2\pi A\cos\gamma}{\beta_s t_{d0}}\right).$$

We call this case "small nonlinearity".

If the soil is allowed to undergo permanent strains due to wave passage of incident waves in the full space, then we may choose the maximum strain:

$$\varepsilon_m < \max\left(\frac{\pi A\sin\gamma}{\beta_s t_{d0}};\frac{\pi A\cos\gamma}{\beta_s t_{d0}}\right).$$

This condition guarantees that in either the x or y direction the soil will undergo permanent strains during the passage of the plane wave.

Generally, the yielding strain can be written as

$$\varepsilon_m = \frac{Cv_{\max}}{\beta_s} = \frac{C\pi A}{\beta_s t_{d0}}, \tag{12}$$

where C is a constant that controls the yielding stress (strain) in the soil. We then consider the following cases of nonlinearity, depending upon C (see Appendix):

– $C \geq 2$: Small nonlinearity. Permanent strain does not occur until the wave hits the foundation.

– $1 \leq C \leq 2$: Intermediate nonlinearity. Permanent strain does not occur until the wave is reflected from the free surface or is scattered from the foundation. Permanent strain will or will not occur after the reflection of the incident wave from the free surface, depending upon the angle of incidence.

– $C < 1$: Large nonlinearity. Permanent strain occurs after reflection from the free surface. Permanent strain may or may not occur before the wave reflects from the foundation surface.

ENERGY DISTRIBUTION IN THE SYSTEM

The energy flow through a given area can be defined, in terms of a plane-wave approximation (Aki & Richards, 1980), as:

$$E_{in}^a = \rho_s \cdot \beta_s \cdot A_{sn} \int_0^{t_{d0}} v^2 \cdot dt \tag{13}$$

where ρ_s and β_s are the density and shear-wave velocity in the soil and v is a particle velocity, which for the excitation considered in this paper is given by Eq. (10). A_{sn} is the area (normal to the direction of the ray) through which the wave is passing. For our geometrical setting (Fig. 1), the area normal to the wave passage is:

$$A_{sn} = 2 \cdot H_m \cdot \sin\gamma + L_m \cdot \cos\gamma = \\ = L_m \cdot (\sin\gamma + \cos\gamma). \tag{14}$$

Inserting Eqs. (10) and (14) into (13) and integrating, the analytical solution for the input wave energy into the model is

$$E_{in}^a = \rho_s \cdot \beta_s \cdot L_m \cdot (\sin\gamma + \cos\gamma) \cdot \left(\frac{\pi A}{t_{d0}}\right)^2 \cdot \frac{t_{d0}}{2} \tag{15}$$

As can be seen from Eq. (15), for the defined size of the soil island, L_m, and the defined angle of incidence, γ, the input energy is reciprocal with the duration of the pulse, which means it is a linear function of the dimensionless frequency η. Because the short pulses in our example calculations are low-pass filtered up to $\omega_c = 200$ rad/s, the analytical and the numerical solutions (13) for input wave energy will not coincide.

Since our system is conservative, the input energy is balanced by:

– Cumulative energy going out from the model, E_{out}, computed using Eq. (13)

– Cumulative hysteretic energy (energy spent for creation and development of permanent strains in the soil), computed from:

$$E_{hys} = \sum_{t=0}^{T_{end}} \Delta t \cdot \sum_{i=1}^{N} \left[\sigma_{xi}(\Delta\varepsilon_{xpi} + 0.5 \cdot \Delta\varepsilon_{xei}) + \sigma_{yi}(\Delta\varepsilon_{ypi} + 0.5 \cdot \Delta\varepsilon_{yei}) \right] \tag{16}$$

where:

T_{end} – is the time at the end of the analysis; N is the total number of points;

σ_{xi}, σ_{yi} – are the stresses at the point i in the x and y directions, respectively;

$\Delta\varepsilon_{xpi} = \varepsilon_{xpi}^{t+\Delta t} - \varepsilon_{xpi}^{t}$ – is the increment of the permanent strain in the x direction at point i; and

$\Delta\varepsilon_{ypi} = \varepsilon_{ypi}^{t+\Delta t} - \varepsilon_{ypi}^{t}$ – is the increment of the permanent strain in the y direction at point i.

– Instantaneous energy in the building, consisting of kinetic and potential energies, which can be computed from:

$$E_b = E_k + E_p = 0.5 \cdot \Delta x \cdot \Delta y_b \cdot \\ \cdot \sum_{i=1}^{N} \left[\rho \cdot v_i^2 + \mu \cdot (\varepsilon_x^2 + \varepsilon_y^2) \right] \tag{17}$$

This balance is described in Gičev (2008) for a semicylindrical foundation, a pulse with $\eta = 1.5$, for incident angle $\gamma = 30°$, and a yielding strain defined by C = 1.5 (Eq. 12), and it will be assumed to hold here as well for the rectangular foundation.

To study only the effect of scattering from the foundation, following Gičev (2008) the building will be con-

sidered to be high enough so that the reflected wave from the top of the building cannot reach the building-foundation contact during the time of analysis. The analysis is terminated when the wave completely exits the soil island. In this paper, the hysteretic energy in the soil and the energy in the building are the subjects of interest. Gičev (2008) studied these two types of energy as functions of the dimensionless frequency η. For a semi-circular foundation, he showed that as the foundation becomes stiffer, a larger part of the input energy is scattered, and less energy enters the building.

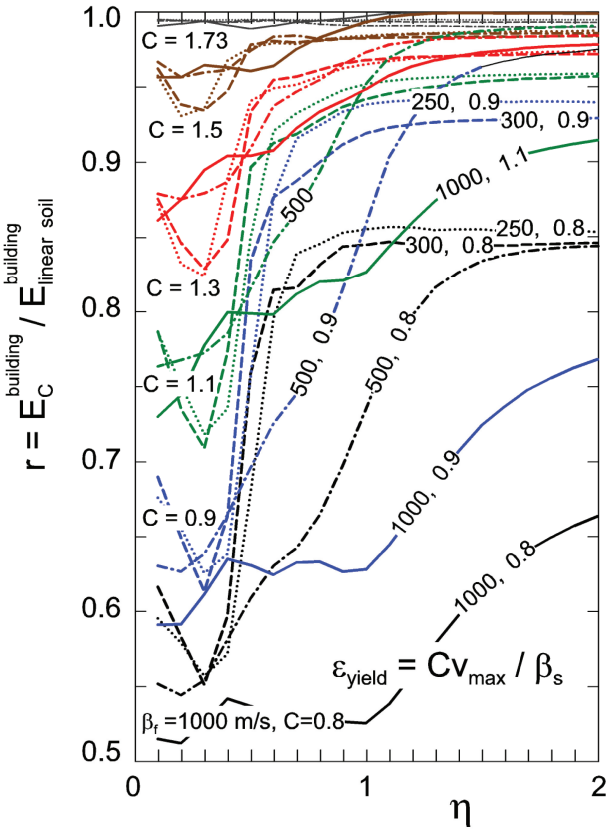

Fig. 3. Reduction of wave energy entering the linear building and linear foundation for different levels of soil nonlinearity (C = 0.8, 0.9, 1.1, 1.3, 1.5, and 1.73) and for different foundation rigidities expressed via β_f = 250, 300, 500, and 1000 m/s.

Figure 3 shows the reduction of the energy entering the building relative to the case of linear soil. The results are shown for four different foundation stiffnesses expressed via β_f = 250, 300, 500, and 1000 m/s. If the soil is linear, the reduction multiplier would be 1. In this figure, we illustrate the energy reduction for six values of C = 0.8, 0.9, 1.1, 1.3, 1.5, and 1.73, as follows. (1) For small nonlinearity (e.g., C = 1.73), the ratios

$$E_C^{building}\ \mathrm{C}=1.73 \,/\, E_{linear\ soil}^{building}\ (\mathrm{C}=\infty)$$

are close to one for every η, showing that the small nonlinearity in the soil does not reduce the energy entering the building significantly. (2) For intermediate nonlinearity (e.g., C = 1.5), the ratios

$$E_C^{building}\ \mathrm{C}=1.5 \,/\, E_{linear\ soil}^{building}\ (\mathrm{C}=\infty)$$

show that there is a small reduction of the energy entering the building with the smallest ratio r ~ 0.94 near η = 0.2 to 0.3 and for β_f = 250 m/s. The values of η = 0.2 to 0.3 correspond to the excitation with wavelengths 3 to 5 times longer than the width of the foundation, and this corresponds to the cases in which all points along the contact of soil and foundation are forced to move in phase and with similar amplitudes. With increasing η (larger than ~0.7), the reduction decreases and the ratio r tends towards 1. (3) For big nonlinearity (e.g., C = 0.8), the ratios

$$E_C^{building}\ \mathrm{C}=0.8 \,/\, E_{linear\ soil}^{building}\ (\mathrm{C}=\infty)$$

show that the reduction of energy entering the building is significant for all considered values of foundation stiffness. The ratio r is the smallest for the stiffest considered foundation (β_f = 1000 m/s).

The results computed for case (3) above are dependent upon the size of the model box. Before the wave reaches the foundation, it loses energy due to work spent for creation of permanent strains in the soil. But for our examples, this dependence turns out to be small. For example, for β_f = 250 m/s and η = 0.3, the case of linear soil gives $E_c^{building}$ (C = 0.8) = 164540 J. For soil box L_m = 10a wide and H_m = 5a deep, the energy entering the building is 90769 J, and the ratio r = 0.55. For a soil box

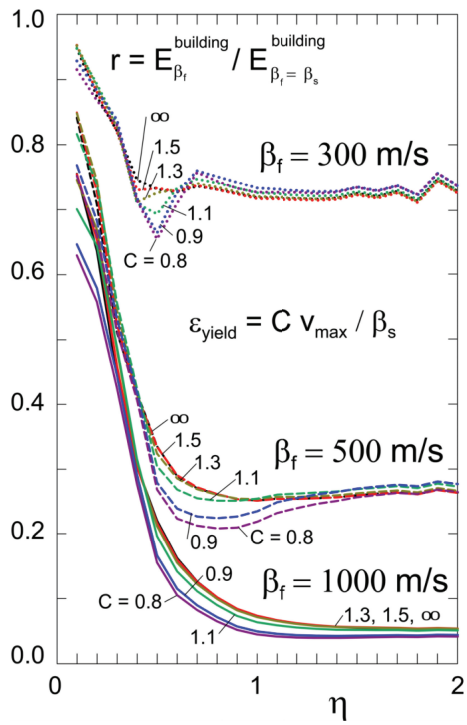

Fig. 4. Reduction of wave energy entering the linear building and linear foundation by scattering, for different levels of soil nonlinearity (C = 0.8, 0.9, 1.1, 1.3, 1.5, and ∞) and for different foundation rigidities expressed via β_f = 300, 500, and 1000 m/s.

$L_m = 20a$ wide and $H_m = 10a$ deep, the energy entering the building is 88884 J, and r = 0.54, which is about a 2% difference for an approximately 2 x 2 smaller soil box. From this, one can conclude that if this extreme case gives only a 2% difference, at other values of η we will obtain even smaller differences due to different sizes of the model. However, if C becomes smaller (for larger nonlinearities) the dependence on the model size will become more pronounced.

Next, we illustrate how the level of the nonlinearity affects the level of scattering. This is shown in Fig. 4. It is seen that the scattering does not depend much on the level of nonlinearity in the soil for small and intermediate nonlinearities and is essentially the same as in the case of linear soil. For large nonlinearity, the effect becomes more significant. The examples in Fig. 4 show that the stiffness of the foundation is the key factor, which determines how much energy is scattered from the foundation.

Figure 5 illustrates the permanent displacements (left) and strains (right) in the soil for nonlinear soil, linear foundation, and linear building SSI. It shows permanent displacements and strains in soils with: small (C = 1.73), intermediate (C = 1.5) and large nonlinearity (C = 0.8). The angle of incidence is $\gamma = \pi/6$, the amplitude of the pulse is A = 0.05m, and the dimensionless frequency is $\eta = h_f/(\beta_s t_d) = 1.5$. The properties for the three media (SH wave velocity, density, width, height) are: in nonlinear soil (250 m/s, 2000 kg/m³, ∞, ∞), yielding strain $\varepsilon_y = Cv_{\max}/\beta_s$; in a linear rectangular foundation (500 m/s, 2000 kg/m³, 19.1 m, 9.55 m), where h_f is foundation height; and in a linear building (100 m/s, 270 kg/m³, 19.1 m, 20.03 m). For small and intermediate nonlinearities, both displacements and strains are asymmetric relative to the foundation. Along the model boundaries (four columns and four rows in the FD mesh), both displacements and strains decrease due to gradual transition from nonlinear to linear material properties in the model.

DISTRIBUTION OF THE PERMANENT STRAIN IN THE SOIL

From dynamic equilibrium of the differential pentahedron (Fig. 6), we can find the principal stress at a point and its direction as $\tau_{zp} = \tau_{zx} \cos\gamma + \tau_{zy} \sin\gamma$ and $\gamma = \tan^{-1}(\tau_{zy}/\tau_{zx})$, respectively. In Figs. 7a,b,c, the principal permanent strain in the soil is illustrated for the case of small nonlinearity (C = √3) for two angles of incidence, γ = 30° and 60°, and for three shear-wave velocities in the foundation, β_f = 250 m/s, 500 m/s, and 1000 m/s. This value of C guarantees that for angles of incidence $30° \le \gamma \le 60°$ there is no occurrence of permanent strain until the

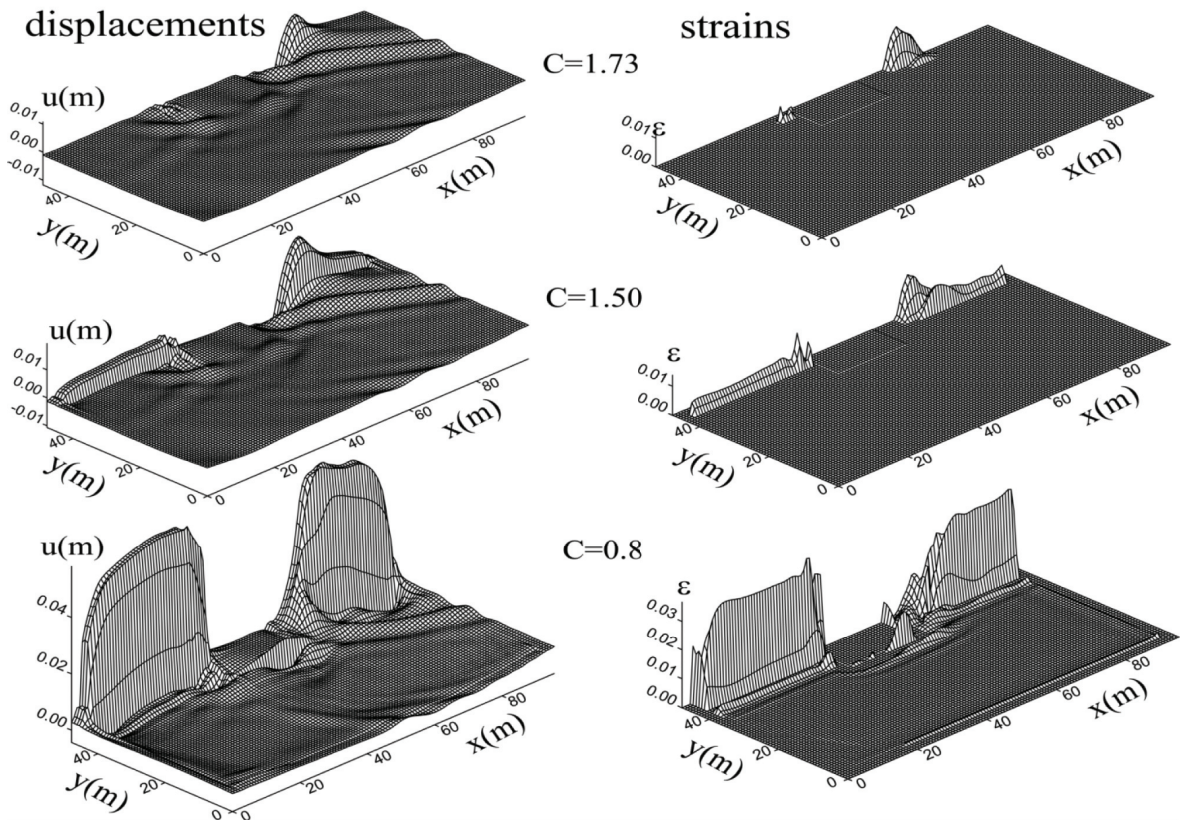

Fig. 5. Permanent displacements (left) and strains (right) in the soil for small (C = 1.73), intermediate (C = 1.5), and large nonlinearity (C = 0.8). The angle of incidence is $\gamma = \pi/6$, the amplitude of the pulse is A = 0.05m, and the dimensionless frequency is $\eta = h_f/(\beta_s t_d) = 1.5$. The properties of the three media (SH wave velocity, density, width, height) are: nonlinear soil (250 m/s, 2000 kg/m³, 95.5 m, 47.75 m), yielding strain $\varepsilon_y = Cv_{max}/\beta_s$; linear rectangular foundation (500 m/s, 2000 kg/m³, 19.1 m, 9.55 m), where h_f is foundation height; linear building (100 m/s, 270 kg/m³, 19.1 m, 20.03 m).

wave hits the foundation. For the wave arrival from the left, upon reflection from the foundation, the nonlinear zones form in the soil along its left wall. The amplitudes of permanent strains increase for reflections from stiffer foundations. With increasing η (shorter wavelengths) the pockets of nonlinear permanent strains become more concentrated and also start to appear in the shadow zone behind the foundation.

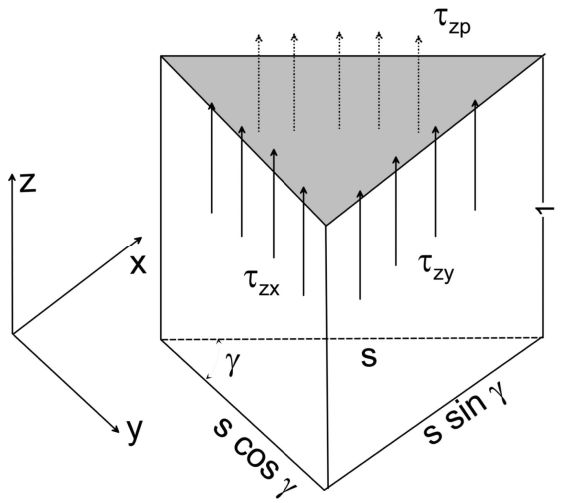

Fig. 6. Orthogonal and principal shear stresses on differential pentahedron.

In Figs. 8a,b,c, the principal permanent strain is illustrated for the case of intermediate nonlinearity (C = 1.5) for the same angles of incidence, γ = 30° and 60°, and for three values of foundation stiffness, β_f = 250, 500, and 1000 m/s. In this case, permanent strain occurs before the wave hits the foundation, but after it reflects from the free surface.

For long pulses η = 0.1, it can be seen from Fig. 7a that for an angle of incidence γ = 30° there is a small, permanent strain for the stiffest foundation (β_f = 1000 m/s) only, while for softer foundations the soil remains linear after the pulse has left the model. For intermediate nonlinearity, shown in Fig. 8a, for an angle of incidence γ = 30° it can be seen that after the creation of nonlinear zones the contribution of the SSI to creation of permanent displacements and strains is negligible relative to the effects of interference of the incoming wave and the reflected wave from the free surface.

This is not the case for γ = 60°. From Figs. 7a and 8a, it can be concluded that for stiffer foundations the effect of interaction is more dominant than the effect of the interference. For the softest considered foundation, the effect of the interaction on creation of nonlinear strains is small.

The observations are similar for a five-times-shorter pulse, η = 0.5. It can be seen from Figs. 7b and 8b that for the softest foundation the effect of the interaction is negligible and that as the foundation becomes stiffer the

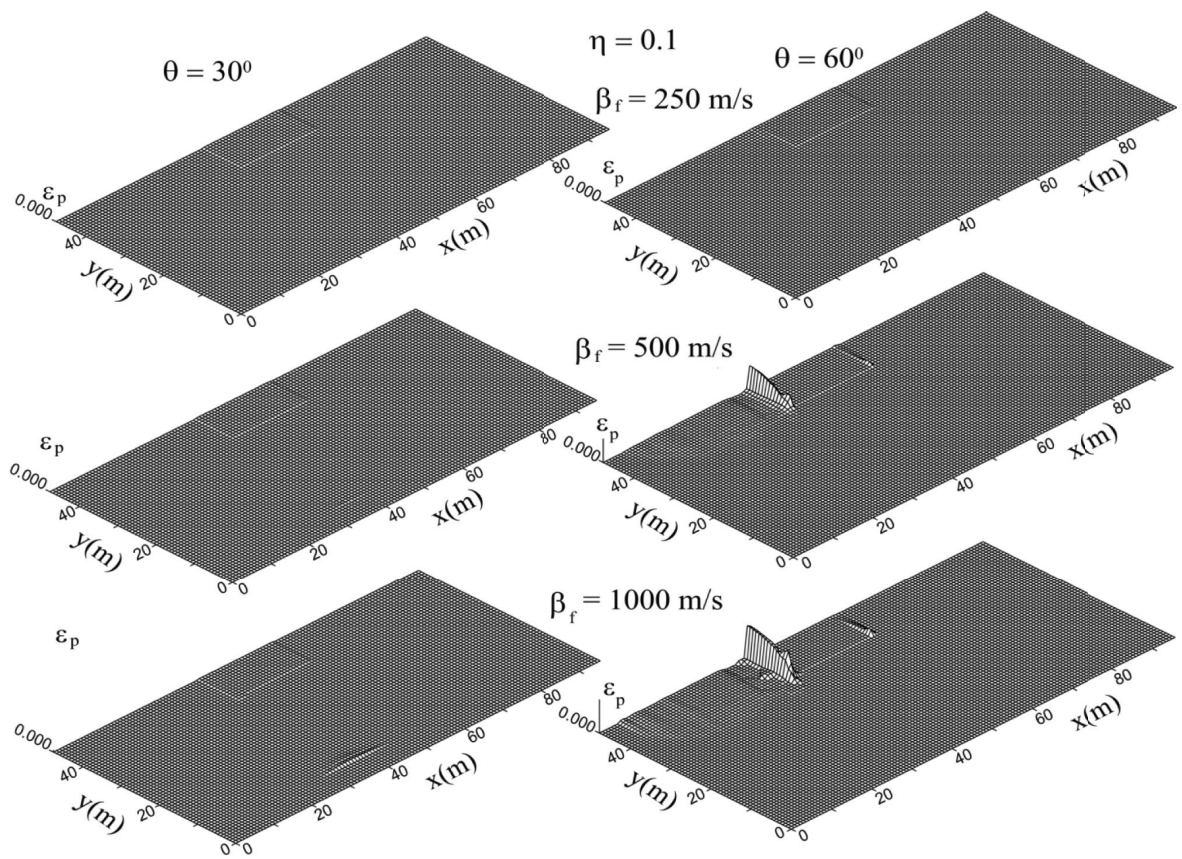

Fig. 7a. Principal permanent strain in the soil for η = 0.1, two angles of incidence, three foundation stiffnesses, and small nonlinearity C = 1.73.

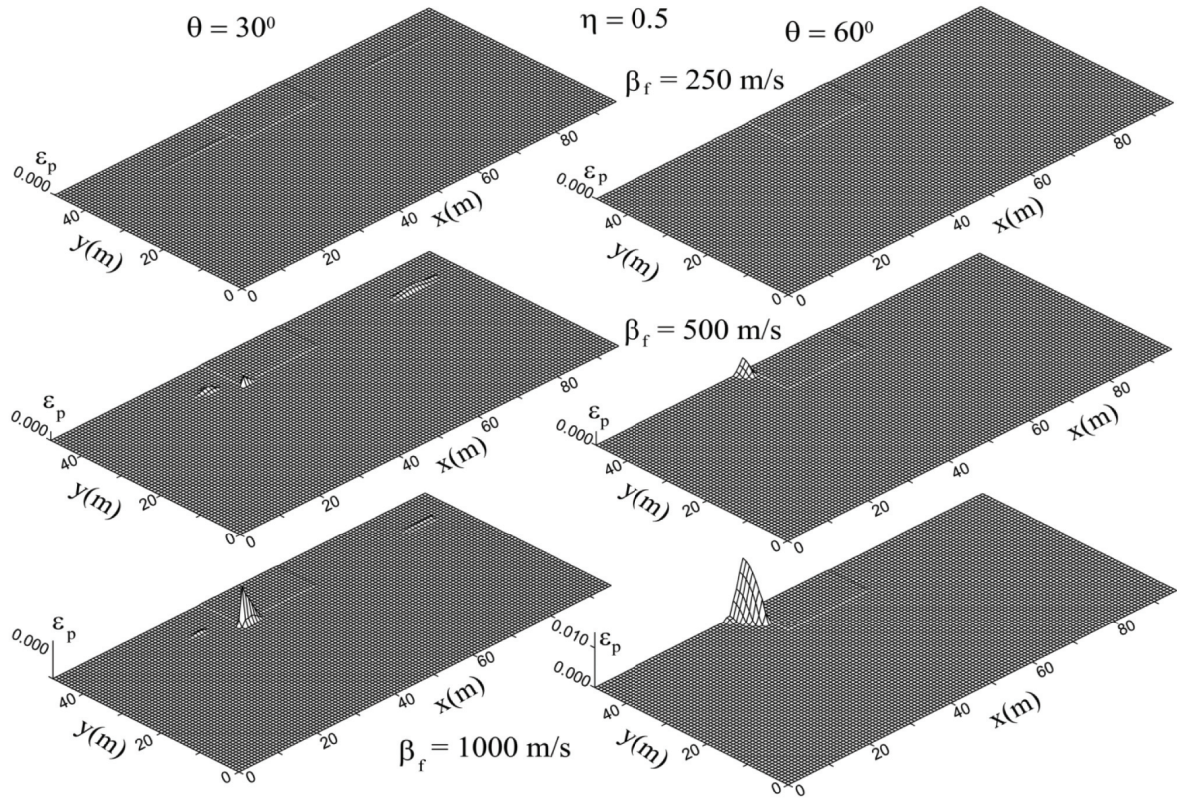

Fig. 7b. Principal permanent strain in the soil for η = 0.5, two angles of incidence, three foundation stiffnesses, and small nonlinearity C = 1.73.

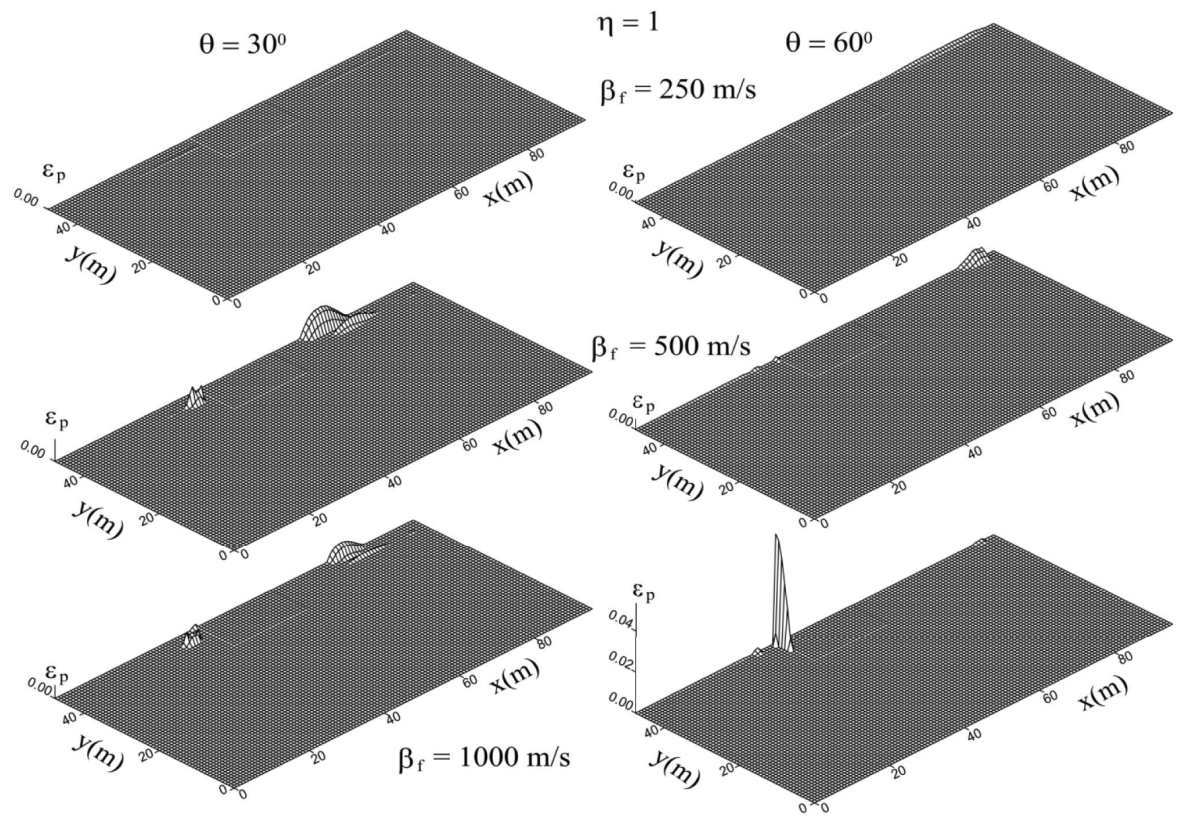

Fig. 7c. Principal permanent strain in the soil for η = 1, two angles of incidence, three foundation stiffnesses, and small nonlinearity C = 1.73.

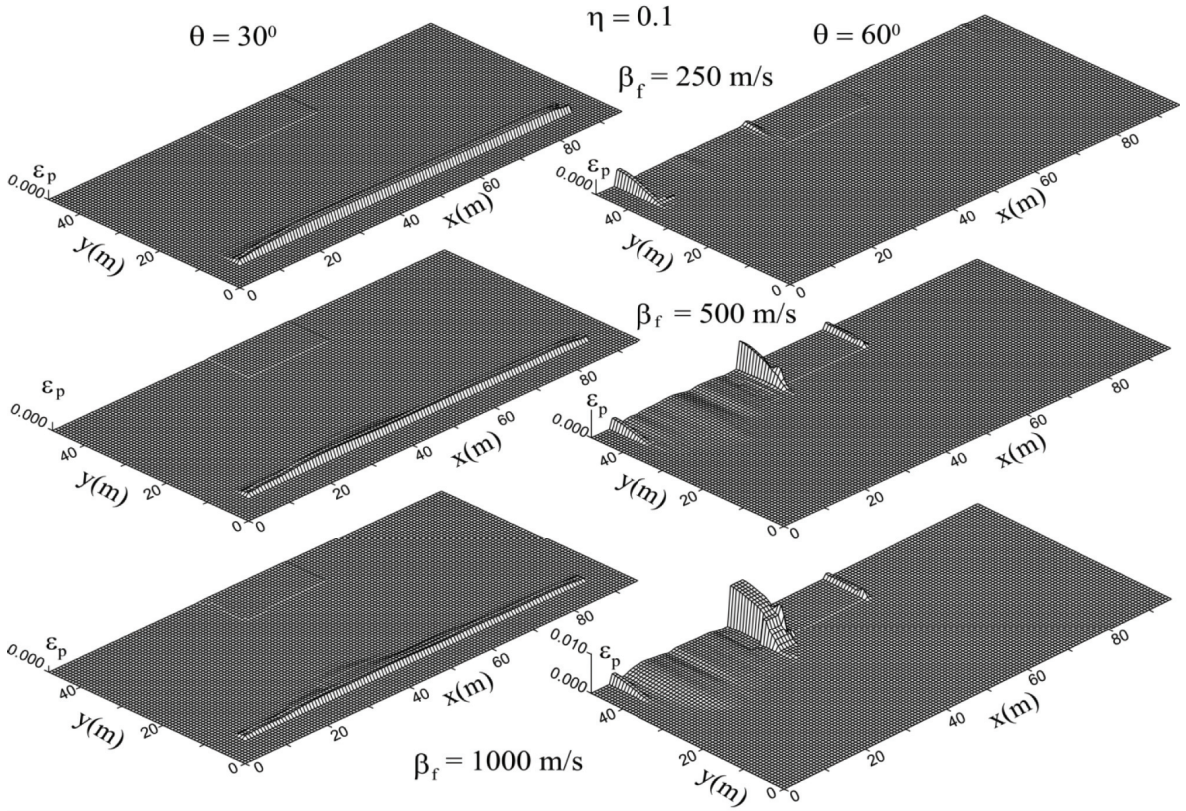

Fig. 8a. Principal permanent strain in the soil for η = 0.1, two angles of incidence, three foundation stiffnesses, and intermediate nonlinearity C = 1.5.

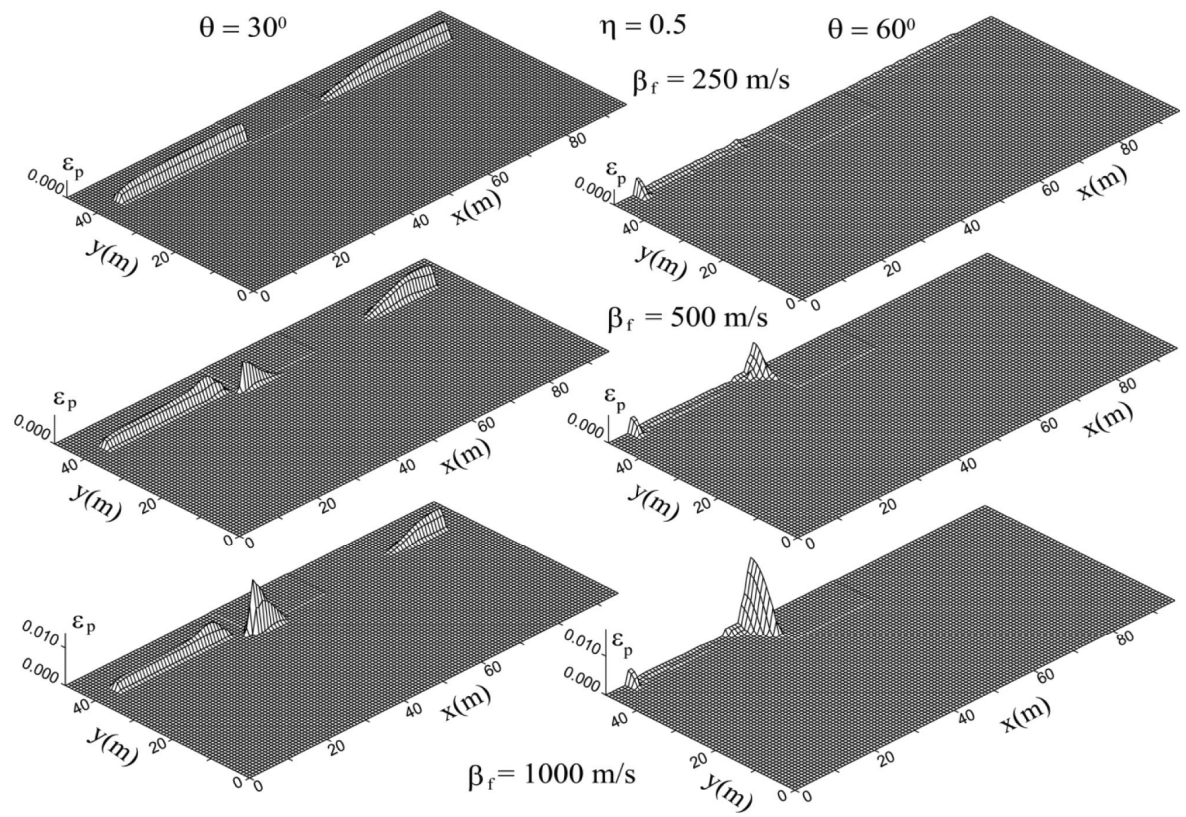

Fig. 8b. Principal permanent strain in the soil for η = 0.5, two angles of incidence, three foundation stiffnesses, and intermediate nonlinearity C = 1.5.

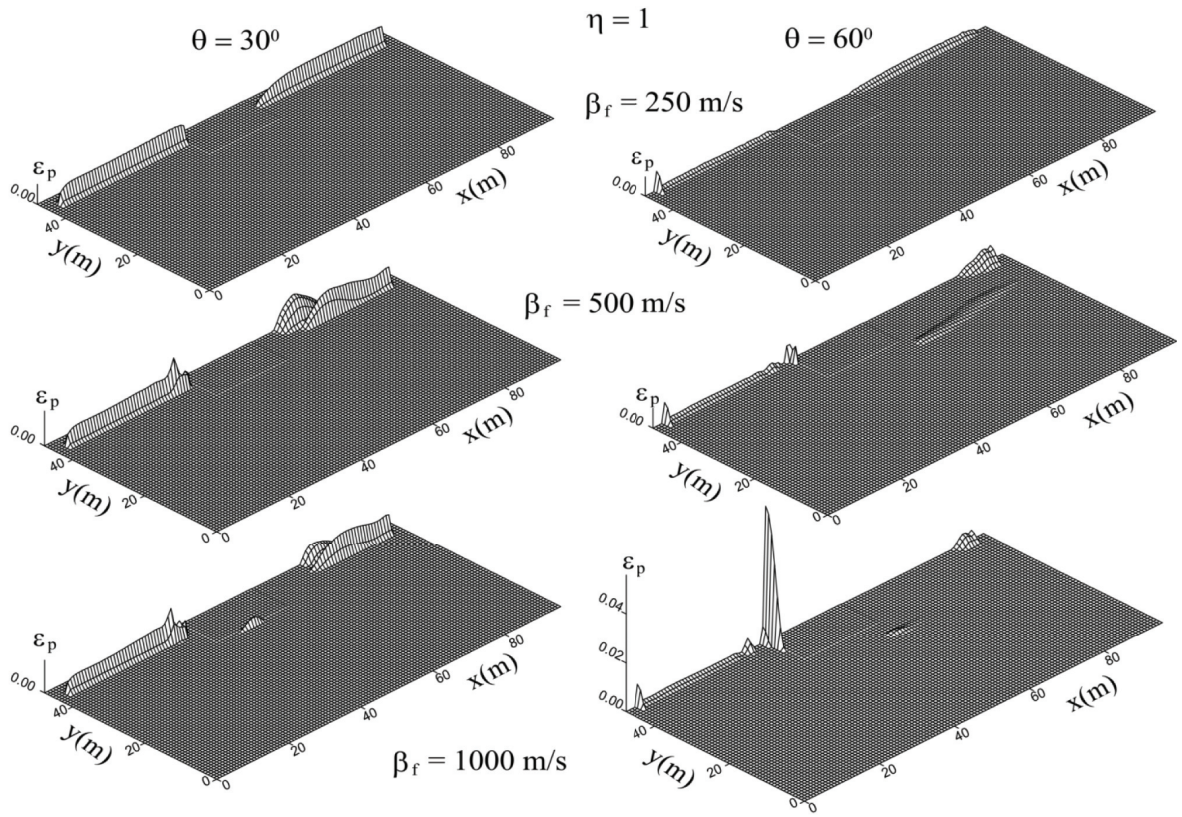

Fig. 8c. Principal permanent strain in the soil for η = 1, two angles of incidence, three foundation stiffnesses, and intermediate nonlinearity C = 1.5.

nonlinear zones are created and developed in the soil next to the front of the foundation.

As the pulse becomes shorter, $\eta = 1$, the nonlinear zones are also formed behind the foundation. This can be explained by the interference of waves reflected from the free surface and diffracted around the foundation, and by the stronger excitation of the soil behind the foundation resulting from more "rigid" forced motion of the foundation by the waves moving its left side. Again, the permanent strain in front of the foundation increases as the stiffness of the foundation increases.

FLEXIBLE FOUNDATION

Flexibility of the foundation results in the wave passage and differential excitation of the building along the horizontal building foundation interface and thus changes the 1D building response for the rigid foundation models into the 2D building response (Trifunac et al. 1999b).

Detailed analysis of the consequences of the flexible foundation on the response of the building and of the associated phenomena is beyond the scope of this paper. We illustrate it here briefly for better and more complete understanding of the results in this paper.

In Fig. 9 we show the displacement at two corners and at mid-point of the building foundation interface (points A, B and C), for incident pulse with amplitude A_{pulse} = 0.05 m, dimensionless frequency η = 0.5, incident angle γ = 30º and for medium properties beneath

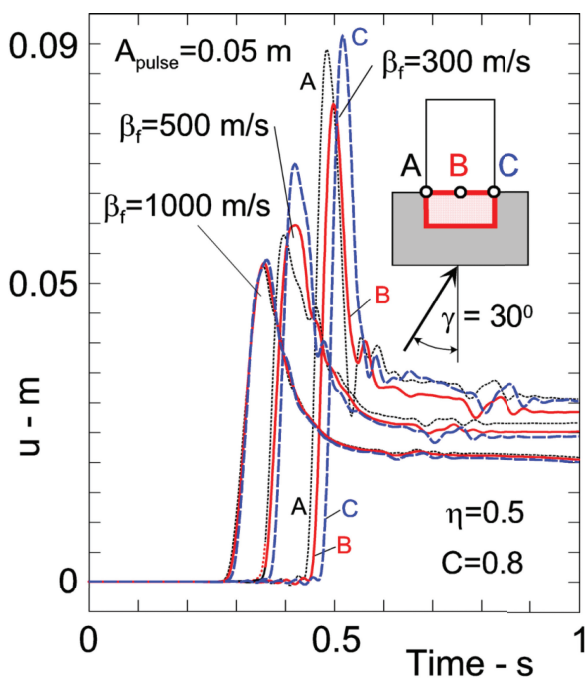

Fig. 9. Displacement at three points in the foundation-building interface for incident strong motion pulse with γ = 30º, for dimensionless frequency of the incident pulse η = 0.5 and for the largest nonlinear response in the soil considered in this paper (C = 0.8). Results are shown for three rigidities of the foundation expressed via β_f = 300, 500 and 1000 m/s.

the foundation, which are associated with large nonlinear soil response before the pulse reaches the foundation (C = 0.8). In Fig. 9 we show motions at A (dotted lines), B (solid lines) and C (dashed lines), and for three foundation rigidities expressed via shear wave velocity in the foundation (β_f = 300, 500 and 1000 m/s). It is seen that for all foundation rigidities the base of the building experiences permanent displacements due to the permanent deformations in the soil.

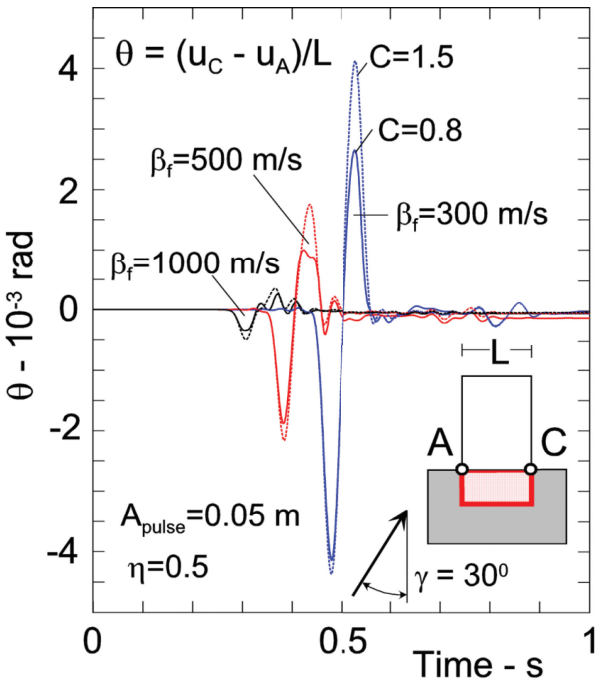

Fig. 10. Cord rotations, between the points A and C on the building-foundation interface, for intermediate nonlinearity (C = 1.5) and for large for nonlinearity in the soil (C = 0.8, for motions shown in Fig. 9).

The 1D nature of the building response on the rigid foundation eliminates the possibility to excite torsion in the building (rotation about the vertical y– axis in Fig. 1) due to wave passage effects, and for all incident angles of the wave, γ .

However, the wave passage along the base of the building for flexible foundation deforms the building as the wave propagates along the foundation width. For long waves, this excitation of the building can be viewed as out of plane motion combined with torsion of the base.

We illustrate this by computing the cord rotation between the two corner points at the base of the building (points A and C in Fig. 9). We show this cord rotation versus time in Fig. 10. As would be expected this "torsion" becomes small and approaches zero as β_f increases. For the model parameters chosen in this paper, this torsion also decreases with increasing nonlinearity in the soil response, and is largest for linear soil response.

The wave passage along the base of the building will increase the vertical strains, at the base of the building, particularly near corners (points A and C) and will result in their time and space variations. This increase will depend on the relative stiffness of the building in translation and in torsion, and on the horizontal wave length of the motion propagating from the foundation into the building (Todorovska and Trifunac 1989, 1990). A related discrete model of a rigid "building" on multiple columns suggests that this amplification can be considerable (Jalali and Trifunac 2011).

We illustrate this qualitatively in Figs. 11 and 12, at the time when the wave begins to enter the building. In Fig. 12 we show the amplitudes of vertical strain in a narrow zone above and bellow the building foundation interface, for the displacements illustrated in Fig. 11. It is seen that while the presence of nonlinear response in the soil, and scattering of incident waves from the flexible foundation contribute to the reduction of seismic wave energy entering the building, the building excitation and its response become more complex and require analysis in terms of more degrees of freedom.

CONCLUSIONS

Numerical methods are powerful tools for studying nonlinear soil-structure interaction problems. Because of grid dispersion, the selection of the grid spacing must be done carefully. Short waves cannot be reconstructed even with very fine grids, and the incident wave (pulse) should be low-pass filtered to utilize numerical methods effectively.

In the presence of a foundation and small angles of incidence (close to vertical incidence), the permanent strains in the y direction are dominant, while for large angles of incidence (close to horizontal incidence) the permanent strains in the x direction are dominant.

For long waves and small angles of incidence (Figs. 7a and 8a for $\theta = 30$), the effect of the interaction on the nonlinear response in the soil is small. For soft foundations, β_f = 250 m/s, and small incident angles (the top left plots in Figs. 7a,b,c and 8a,b,c), the effect of the interaction on the nonlinear response of the soil is also small. As the foundation becomes stiffer, zones of large permanent strains develop around the foundation.

For stiff foundations, short waves and large incidence angles, a zone of permanent strains develops behind the foundation, which appears to be due to the concentration of rays associated with diffraction of the waves from the foundation.

The zones of large permanent strains illustrated in Figs. 7a,b,c and 8a,b,c are responsible for the damage and failures in the shallow infrastructure (water and gas pipes, underground cables, etc.) that accompany large earthquakes and cause interruptions of gas and water supplies (Trifunac and Todorovska 1997a, 1998).

As the large and permanent strains develop along the foundation-soil interface, the effective foundation compliances are reduced, which in turn decreases the equivalent rocking stiffness of the foundation-structure system.

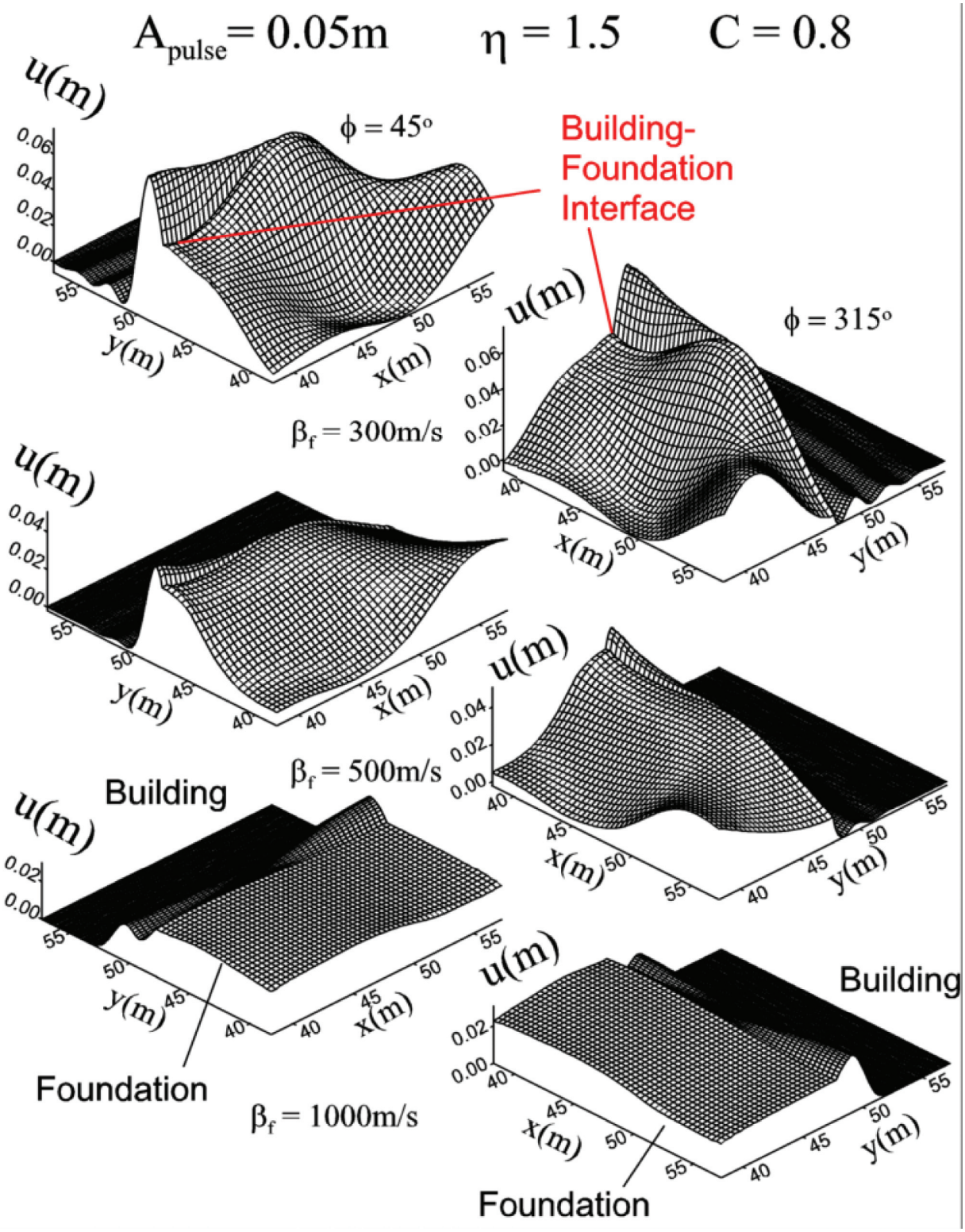

Fig. 11. Displacements in the foundation and in the lower portion of the building, for short strong motion pulse (η = 1.5) and large nonlinear response in the soil (C = 0.8), for different rigidities of the foundation expressed via shear wave velocity (β_f = 300, 500 and 1000m/s). Two views are shown for φ = 45° and 315°, measured clockwise from the vertical axis pointing down.

With simultaneous action of in-plane wave motions, which are always present in 3D settings during earthquake excitation and which will excite the in-plane rocking of the model, it is easy to see how the nonlinear zones in the soil (as illustrated in Figs. 7 and 8) will take the structure one step closer to overturning and eventual collapse, as in the examples mentioned in the introduction.

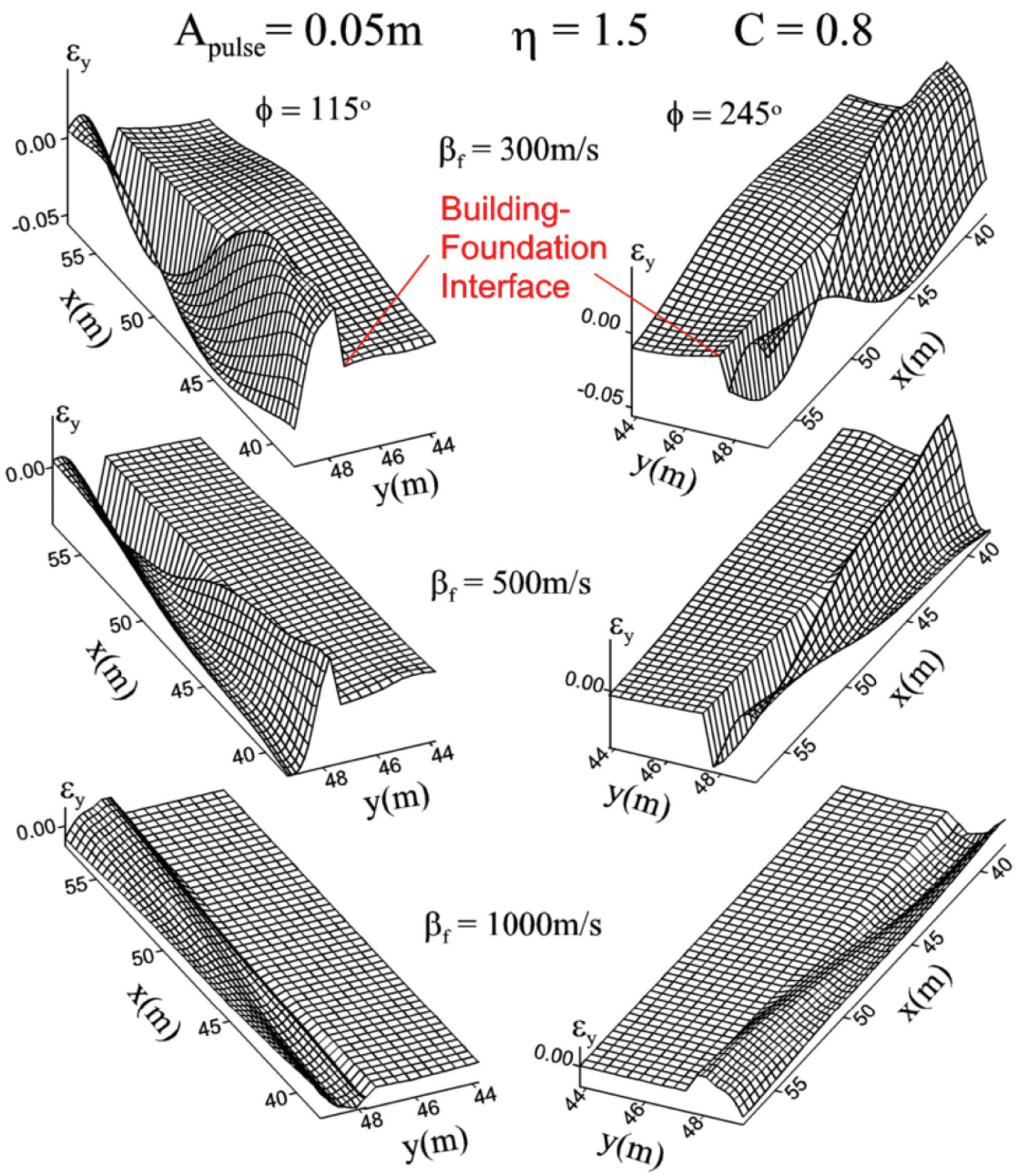

Fig. 12. Distribution of vertical strains ε_y in the narrow strips above and bellow the building foundation interface, for $\eta = 1.5$ and large nonlinear response in the soil ($C = 0.8$), for different rigidities of the foundation expressed via shear wave velocity ($\beta_f = 300$, 500 and 1000m/s). Two views are shown for $\phi = 115°$ and 245°, measured clockwise from the vertical axis pointing down.

APPENDIX

The motion of the plane SH wave pulse in the full space can be written as:

$$w = A\sin\left[\frac{\pi}{t_d}\cdot\left(t-\frac{l}{\beta}\right)\right]\cdot \left[H\left(t-\frac{l}{\beta}\right)-H\left(t-\frac{l}{\beta}-t_d\right)\right] \quad \text{(A.1)}$$

where l is the coordinate along the direction of propagation, β is the shear wave velocity, and H is the Heaviside (step) function.

Considering the motion in the x and y directions (phase motions), and dividing l and β in (A.1) by $\sin\gamma$ (where γ is the angle of incidence), we get the phase motion in the x direction:

$$w = A\sin\left[\frac{\pi}{t_d}\cdot\left(t-\frac{x}{c_x}\right)\right]\cdot \left[H\left(t-\frac{x}{c_x}\right)-H\left(t-\frac{x}{c_x}-t_d\right)\right]$$

If we omit the second multiplier (= 1 corresponding with the interval when the pulse occupies the considered

point) and take the derivative with respect to space coordinate x, we get the strain in the x direction:

$$\varepsilon_x = \frac{\pi \cdot A \cdot \sin\gamma}{\beta \cdot t_d} \tag{A.2a}$$

In the same way we get the strain in the y direction:

$$\varepsilon_y = \frac{\pi \cdot A \cdot \cos\gamma}{\beta \cdot t_d} \tag{A.2b}$$

The strains (A.2a) and (A.2b) are strain components for full space. To get the peak strains from half-sine pulse motion in half space, we add the contributions from the incoming and reflected pulse from the half space. The peak strain in the x direction occurs at the free surface. The reflected strain does not change the sign, and the resultant peak strain is just double the strain in (A.2a):

$$\varepsilon_x = \frac{2 \cdot \pi \cdot A \cdot \sin\gamma}{\beta \cdot t_d} \tag{A.3a}$$

The peak strain in the y direction occurs at some distance below the free surface. The reflected strain changes the sign, and its maximum amplitude occurs when the front of the reflected (max positive) and the tail of the incoming (max positive) strain meet. The resultant peak strain is again double the strain in (A.2b):

$$\varepsilon_y = \frac{2 \cdot \pi \cdot A \cdot \cos\gamma}{\beta \cdot t_d} \tag{A.3b}$$

If we write the yielding strain as:

$$\varepsilon_{yield} = C\frac{\pi \cdot A}{\beta \cdot t_d} \tag{A.4}$$

it can be seen from (A.3a) and (A.3b) that if $C \geq 2$, for any angle of incidence γ, neither ε_x nor ε_y will reach ε_{yield} in the half space. The yielding strain ε_{yield} may be reached only due to scattering from foundation and soil-structure interaction (SSI) effects. This case, when the x and y components of the strain in the half space are smaller than the yielding strain, we call small nonlinearity.

From (A.3a) and (A.3b), it is seen that for $\pi/6 \leq \gamma \leq \pi/3$ neither ε_x nor ε_y will reach ε_{yield} for

$$C = 2\cos\frac{\pi}{6} = 2\sin\frac{\pi}{3} = \sqrt{3}$$

Because in this paper we consider angles of incidence $\gamma = \pi/6$ and $\gamma = \pi/3$, we take $C = \sqrt{3}$ as an example of small nonlinearity. We choose this C to point out the permanent strains created and developed due to SSI. For this C, there is no permanent strain due to interference of reflected and incoming waves.

For $1 \leq C \leq 2$, we have the case of intermediate nonlinearity, when either ε_x or ε_y or both exceed ε_{yield} after reflecting from the half space for any angle of incidence. In the interval of incident angles, $\pi/6 \leq \gamma \leq \pi/3$, the interval of C for intermediate nonlinearity is

$$\sqrt{3}/2 \leq C \leq \sqrt{3}.$$

For $C \leq \sqrt{3}/2$, we have the case of large nonlinearity, when either ε_x or ε_y or both exceed ε_{yield} even before the wave is reflected from the free surface.

REFERENCES

[1] Aki, K., & Richards, P. (1980). *Quantitative seismology, theory and methods*. Publication: W.H. Freeman & Co.

[2] Alford, R.M., Kelly, K.R., & Boore, D.M. (1974). Accuracy of finite-difference modeling of the acoustic wave equation. *Geophysics, 39*, 834–842.

[3] Alterman, Z., & Karal, F.C. (1968). Propagation of elastic waves in layered media by finite difference methods. *Bull. Seism. Soc. of Amer., 58* (1), 367–398.

[4] Aviles, J., Suarez, M., & Sanchez–Sesma, F.J. (2002). Effects of wave passage on the relevant dynamic properties of structures with flexible foundation. *Earthq. Eng. and Struct. Dynamics,* 31, 139–159.

[5] Blume and Assoc. (1973). *Holiday Inn, in San Fernando, California, earthquake of February 9, 1971*. (L.M. Murphy, Ed.). U.S. Dept. of Commerce, National Oceanic and Atmospheric Administration, Washington, D.C.

[6] Boore, D.M. (1972). Finite difference methods for seismic wave propagation in heterogeneous materials. In *Methods in Comp. Physics 11*. New York: Academic Press Inc.

[7] Caballero, F.L., Farahmand-Razavi, A.M. (2008). Numerical simulation of liquefaction effects on seismic SSI, Soil Dynamics and Earthquake Engineering, 28(2), 85-98.

[8] Cai, Y.X., Gould, P.L. and Desai, C.S. (2000). Nonlinear analysis of 3D seismic interaction of soil-pile-structure system and application, Engineering Structures, 22(2), 191-199.

[9] Dablain, M.A. (1986). The application of high-order differencing to the scalar wave equation. *Geophysics,* 51(1), 54–66.

[10] Duke, C.M., 1958, *Bibliography of effects of soil conditions on earthquake damage*. Berkeley, CA: Earthquake Engineering Research Institute.

[11] Elgamal, A., Linjun, Y., Zaohui, Y., and Conte, J.P. (2008). Three-Dimensional Seismic Response of Humboldt Bay Bridge-Foundation-Ground System, *J. of Structural Eng., ASCE,* 134(7), 1165-1176.

[12] Fah D.J. (1992). *A hybrid technique for the estimation of strong ground motion in sedimentary basins*. Dissertation, Swiss Federal Institute of Technology, Zurich, Switzerland.

[13] Gičev, V. (2005). *Investigation of soil-flexible foundation-structure interaction for incident plane SH waves*. Ph.D. Dissertation, Dept. of Civil Engineer-

ing, Univ. Southern California, Los Angeles, California.
[14] Gičev, V. (2008). Soil-structure interaction in nonlinear soil, *Izgradnja,* 62(12), 555-566.
[15] Gičev, V. and Trifunac, M.D. (2007)[1]. Energy and Power of Nonlinear Waves in a Seven Story Reinforced Concrete Building, *Indian Society of Earthquake Technology Journal*, 44(1), 305-323.
[16] Gičev, V. and Trifunac, M.D. (2009). Rotations in a Shear Beam Model of a Seven-Story Building Caused by Nonlinear Waves During Earthquake Excitation, *Structural Control and Health Monitoring*, 16(4), 460-482.
[17] Hayir, A., Todorovska, M.I., & Trifunac, M.D. (2001). Antiplane response of a dike with flexible soil-structure interface to incident SH waves. *Soil Dynam. and Earthq. Eng., 21*, 603–613.
[18] Housner, G.W. and Trifunac, M.D. (1967). Analysis of Accelerograms – Parkfield Earthquake, *Bull. Seism. Soc. Amer.*, 57(6), 1193-1220.
[19] Ivanović, S.S., Trifunac, M.D., Novikova, E.I., Gladkov, A.A., and Todorovska, M.I. (2000). Ambient vibration tests of a seven-story reinforced concrete building in Van Nuys, California, damaged by the 1994 Northridge Earthquake, *Soil Dynamics and Earthquake Engrg*, 19(6), 391-411.
[20] Jalali, R.S. and Trifunac, M.D. (2011). A note on the wave-passage effects in out-of-plane response of long structures to strong earthquake pulses, *Soil Dynamics and Earthquake Eng.,* 31(4), 640-647.
[21] Kanai, K. (1983). *Engineering Seismology*. Tokyo: Univ. of Tokyo Press.
[22] Lax, P.D., & Wendroff, B. (1964). Difference schemes for hyperbolic equations with high order of accuracy. *Comm. on Pure and Applied Mathematics, XVII*, 381–398.
[23] Lee, V.W. (1979)[1)]. *Investigation of three-dimensional soil-structure interaction*. Report No. CE 79–11, Dept. of Civil Engineering, Univ. of Southern California, Los Angeles, CA.
[24] Luco, J.E., & Wong, H.L. (1977). Dynamic response of rectangular foundations for Rayleigh wave excitation. *Proc. 6th World Conf. on Earthq. Eng., Vol. II*, New Delhi, India.
[25] Luco, J.E., Trifunac, M.D. & Wong, H.L. (1987). On the Apparent Changes in Dynamic Behavior of a Nine-story Reinforced Concrete Building, *Bull. Seism. Soc. Amer.*, **77**(6), 1961-1983.
[26] Mitchell, A.R. (1969). *Computational methods in partial differential equations*. New York: John Willey & Sons.
[27] Moczo, P. (1989). Finite-difference technique for SH-waves in 2-D media using irregular grids—application to the seismic response problem. *Geophys. Jour. Int.,* 99, 321–329.
[28] Prevost, J.H. (1993). Nonlinear Dynamic Response Analysis of soil and Soil-Structure interaction systems, Seminar on Soil Dynamics and Geotechnical Earthquake Engineering, Editors: Seco, E. and Pinto, P., *Soil Dynamics and Earthquake Engineering*, Balkema, Rotterdam, 49-126.
[29] Seed, H.B. (1970). Soil problems and soil behaviour, Chapter 10 in *Earthquake Engineering* (Edited by R.L. Wiegel). Englewood Cliffs, NJ, Prentice Hall.
[30] Todorovska, M.I. (2009). Seismic Interferometry of Soil-Structure Interaction Model with Coupled Horizontal and Rocking Response, *Bull. Seism. Soc. of America,* 99(2A), 611-25.
[31] Todorovska, M.I, and Trifunac, M.D. (1989). Antiplane earthquake waves in long structures, J. Eng. Mechanics. ASCE. 115(12), 2687-2708.
[32] Todorovska, M.I. and Trifunac, M.D. (1990). A note on excitation of long structures by ground waves. J. Eng. Mech., ASCE, 116(4), 952-964.
[33] Todorovska, M.I., Hayir, A., & Trifunac, M.D. (2001). Antiplane response of a dike on flexible embedded foundation to incident SH-waves. *Soil Dynam. and Earthq. Eng.,* 21, 593–601.
[34] Todorovska, M.I., Trifunac, M.D. and Lee, V.W. (2007). Shaking Hazard Compatible Methodology for Probabilistic Assessment of Permanent Ground Displacement Across Earthquake Faults, *Soil Dynamics and Earthquake Engineering,* 27(6), 586-597.
[35] Todorovska, M.I., Meidani, H, and Trifunac, M.D. (2009). Wavelet Approximation of Earthquake Strong Ground Motion – Goodness of Fit for a Database in Predicting Nonlinear Structural Response, *Soil Dynamics and Earthquake Engineering*, 29(4), 742-751.
[36] Trifunac, M.D. (1995). Empirical criteria for liquefaction in sands via standard penetration tests and seismic wave energy, *Soil Dynamics and Earthquake Eng*., 14(6), 419–426.
[37] Trifunac, M.D. (2008). Energy of Strong Motion at Earthquake Source, *Soil Dynamics and Earthquake Engineering,* 28(1), 1-6.
[38] Trifunac, M.D. & Gičev, V. (2006). Response Spectra for Differential Motion of Columns, Paper II: Out-of-Plane Response, *Soil Dynamics and Earthquake Engineering*, 26(12), 1149-1160.
[39] Trifunac, M.D. & Ivanović, S.S. (2003a). Reoccurrence of Site Specific Response in Former Yugoslavia – part I: Montenegro, *Soil Dynamics and Earthquake Eng*., 23(8), 637-661.
[40] Trifunac, M.D. & Ivanović, S.S. (2003b). Reoccurrence of Site Specific Response in Former Yugoslavia – Part II: Friuli, Banja Luka and Kopaonik, *Soil Dynamics and Earthquake Eng*., 23(8), 663-681.
[41] Trifunac, M. D. and Lee, V. W. (1996). Peak Surface Strains During Strong Earthquake Motion, *Soil Dynamics and Earthquake Eng*., 15(5), 311-319.

[1)] Can be downloaded from: http://www.usc.edu/dept/civil_eng/Earthquake_eng/

[42] Trifunac, M.D., & Todorovska, M.I. (1989). Antiplane Earthquake Waves in Long Structures, *ASCE, EMD*, 115(2), 2687-2708.
[43] Trifunac, M.D., & Todorovska, M.I. (1996). Nonlinear Soil Response – 1994 Northridge California, Earthquake, *J. of Geotechnical Eng.*, ASCE, 122(9), 725-735.
[44] Trifunac, M.D., & Todorovska, M.I. (1997a). Northridge, California, earthquake of 17 January 1994: Density of pipe breaks and surface strains. *Soil Dynamics and Earthquake Eng*., 16(3), 193–207.
[45] Trifunac, M.D., & Todorovska, M.I. (1997b). Northridge, California, earthquake of 17 January 1994: Density of red-tagged buildings versus peak horizontal velocity and intensity of shaking, Soil Dynamics and Earthquake Engineering, 16(8), 209-222.
[46] Trifunac, M.D., & Todorovska, M.I. (1997c. Response Spectra and Differential Motion of Columns, with M.I. Todorovska, *Earthquake Eng. and Structural Dyn*., 26(2), 251-268.
[47] Trifunac, M.D., & Todorovska, M.I. (1998). Nonlinear soil response as a natural passive isolation mechanism—the 1994 Northridge, California earthquake. *Soil Dynamics and Earthquake Eng*., 17(1), 41–51.
[48] Trifunac, M.D., & Todorovska, M.I. (1999). Reduction of structural damage by nonlinear soil response, *J. of Structural Eng.*, ASCE, 125(1), 89-97.
[49] Trifunac, M.D., Hao, T.Y. & Todorovska, M.I. (1999a). On reoccurrence of site specific response, *Soil Dynamics & Earthquake Engrg*, 18(8), 569-592.
[50] Trifunac, M.D., Ivanović, S.S. & Todorovska, M.I. (2001a). Apparent periods of a building I: Fourier analysis, *J. of Struct. Engrg*, ASCE, 127(5), 517-526.
[51] Trifunac, M.D., Ivanović, S.S. & Todorovska, M.I. (2001b). Apparent periods of a building II: time-frequency analysis, *J. of Struct. Engrg*, ASCE, 127(5), 527-537.
[52] Trifunac, M.D., Ivanović, S.S., and Todorovska, M.I. (2003). Wave propagation in a seven-story reinforced concrete building, Part III: damage detection via changes in wave-numbers, *Soil Dynamics and Earthquake Engrg*, 23(1), 65-75.
[53] Trifunac, M.D., Ivanović, S.S., Todorovska, M.I., Novikova, E.I. & Gladkov, A.A (1999b). Experimental evidence for flexibility of a building foundation supported by concrete friction piles, *Soil Dynamics & Earthquake Engrg*, 18(3), 169-187.
[54] Trifunac, M.D., Todorovska, M.I. & Ivanović, S.S. (1994). A Note on distribution of uncorrected peak ground accelerations during the Northridge, California, earthquake of 17 January 1994, *Soil Dynamics and Earthquake Engineering*, 13(3), 187-196.
[55] Trifunac, M.D., Todorovska, M.I. & Ivanović, S.S. (1996). Peak Velocities, and Peak Surface Strains During Northridge, California, Earthquake of 17 January 1994, *Soil Dynamics and Earthquake Eng*., 15(5), 301-310.
[56] Trifunac, M.D., Ivanović, S.S, Todorovska, M.I., Novikova, E.I. and Gladkov, A. (1999b). Experimental evidence for flexibility of a building foundation supported by concrete friction piles, *Soil Dynamics and Earthquake Engineering*, 18(3), 169-187.
[57] Tsynkov, S.V. (1998). Numerical solution of problems on unbounded domains: A review. *Applied Numerical Mathematics,* 27, 465 – 532.
[58] Udwadia, F.E. & Trifunac, M.D. (1974). Characterization of Response Spectra through the Statistics of Oscillator Response, *Bull. Seism. Soc. Amer.*, 64(1), 205-219.
[59] Westermo, B.D., & Wong, H.L. (1977). On the fundamental differences of three basic soil–structure interaction models. *Proc. 6th World Conf. of Eart. Eng., Vol.II*, New Delhi, India.
[60] Wong, H.L., & Trifunac, M.D. (1974). Interaction of a shear wall with the soil for incident plane SH waves: Elliptical rigid foundation. *Bull. Seism. Soc. of America,* 64(6), 1825–1884.
[61] Wong, H.L., & Trifunac, M.D. (1975). Two-dimensional antiplane, building-soil-building interaction for two or more buildings and for incident plane SH waves. *Bull. Seism. Soc. of America,* 65(6), 1863–1885.
[62] Zahradnik, J., Moczo, P., & Hron F. (1993). Testing four elastic finite-difference schemes for behaviour at discontinuities. *Bull. Seism. Soc. of America,* 83, 107–129.
[63] Zang, Y., Conte, J.P., Yang, Z., Elgamal, A., Bielak, J., and Acero, G. (2008). Two-dimensional Nonlinear Earthquake Response Analysis of Bridge-Foundation-Ground System, Earthquake Spectra, 24(2), 343-386.

[1] Can be downloaded from http://home.iitk.ac.in/~vinaykg/iset.html